ELSEVIER

Biophysical Chemistry 125 (2007) 334–340

Biophysical Chemistry

http://www.elsevier.com/locate/biophyschem

Layer formations in the bacteria membrane mimetic DPPE-DPPG/water system induced by sulfadiazine

Ágnes Oszlánczi [a], Attila Bóta [a,*], Erwin Klumpp [b]

[a] *Department of Physical Chemistry, Budapest University of Technology and Economics H-1521, Budapest, Hungary*
[b] *Agrosphere Institute, Research Centre Jülich D-52425 Jülich, Germany*

Received 16 May 2006; received in revised form 15 September 2006; accepted 18 September 2006
Available online 12 October 2006

Abstract

The effect of the frequently used antibiotic sulfadiazine (SD) was studied on a bacteria membrane mimetic model system by using differential scanning calorimetric (DSC), small- and wide-angle X-ray scattering (SWAXS) and freeze-fracture methods. The membrane model system consisted of dipalmitoylphosphatidylethanolamine (DPPE, 0.8 molar ratio) and dipalmitoylphosphatidylglycerol (DPPG, 0.2 molar ratio). The SD molar ratio (relative to the lipids) was varied between 10^{-3} and 1. In the presence of SD, two transitions between the gel and liquid crystalline phases appear at 60.5 °C and about at 65 °C. In the temperature domain of the gel phase, the subcell of the chain packing is strongly temperature dependent indicating the increased dominance of the hydration forces during the first transition and the location of SD molecules in the neighbourhood of the polar lipid head groups. The second transition is accompanied by the changes in the nanometer-scale layer arrangements observed by SAXS and in the μm-scale morphology observed by freeze-fracture. Above the temperature of the second transition, the SD-induced metastable structures undergo further formations to produce a more homogeneous state favoured by the geometrical packing of the cylindrical-shaped lipid molecules.

Keywords: Sulfadiazine; DPPE-DPPG vesicles; Phase separation; DSC; Small- and wide-angle X-ray scattering (SWAXS); Freeze-fracture

1. Introduction

As a group of antimicrobial medicines, antibiotics kill microorganisms or suppress their multiplication and growth. These substances are used not only as human and veterinary medicines for bacterial infections, but they are also applied as feed additives to prevent infections in livestock, for example at poultry and fish farms, to treat the entire flock or herd at risk [1,2]. These drugs appear in the environment of the treated animals and can also lead to toxic effects in terrestrial and aquatic organisms [3]. Up to now, there has not been any extensive investigation of the pernicious effects of these molecules considering the importance of this risk in the extended application of antibiotics [4].

Sulphonamides are synthetic antimicrobial agents derived from sulfonic acid. These molecules act as competitive inhibitors of para-aminobenzoic acid, which is a necessary intermediate in these organisms for the synthesis of folic acid during DNA synthesis [5]. Sulfadiazine (SD, Fig. 1), a sulpha drug, is one of the most frequently used antibiotics for the therapy of domestic animals and farmed fish [1]. The solubility of sulfadiazine is generally low, but it is higher in water (about 60 mg/dm^3) than in organic solvents [6].

The smallest changes in the membrane composition can influence the membrane processes resulting in minor or even drastic changes in the material transport and in other important (for example: signal) features of cell membranes [7–9]. In spite of the fact that biological membranes consist of a relatively small number of components, the explanation of the effect of antibiotics remains ambiguous because of the complex mechanism of the membranes. Therefore, of the different model systems, vesicles as model membranes are generally studied to

* Corresponding author.
E-mail address: abota@mail.bme.hu (A. Bóta).

0301-4622/$ - see front matter © 2006 Elsevier B.V. All rights reserved.
doi:10.1016/j.bpc.2006.09.008

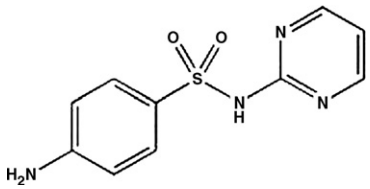

Fig. 1. Sulfadiazine (SD).

obtain information about the effect of toxic molecules like antibiotics on the real membrane structure [10–15].

The typical main phospholipid components of the bacterial membranes are the phosphatidylethanolamines (PEs). For example, PEs are present in the cytoplasmic membrane of *Staphylococcus aureus*, *Escherichia coli*, *Pseudomonas aeruginosa*, *Nitromonas europaea*, and *Salmonella typhimurium*, and therefore these phospholipids are frequently used to prepare biologically relevant vesicles [16]. In general, a higher concentration of DPPE is found in the inner membrane of Gram-negative bacteria as compared to Gram-positive bacteria [17,18]. To obtain reliable structural and thermotropic information on real membranes, mixtures of different lipids are applied in model investigations. In addition to the PEs, the phosphatidylglycerols (PGs) are the most frequently found membrane constituents of Gram-negative bacteria. Indeed, the dipalmitoylphosphatidylethanolamine(DPPE)-dipalmitoylphosphatidylglycerol(DPPG)/water vesicles proved to be the more relevant system than that consisting of only DPPE as was suggested and characterized by Lohner and colleagues [19,20]. The DPPE-DPPG system exhibits several special features and different domain formations appear to depend on the DPPE molar ratio [19]. In our work, the DPPG was added in a 0.2 DPPG/DPPE+DPPG molar lipid ratio to the system to approximate the complexity of the bacteria membranes. In this case, the calorimetric studies indicate an inhomogeneous state with microdomains resulting in a segregation in the system [21,22]. According to the chemical character of SD, it is expected to be located in the water shells of the vesicles. The effects induced by the presence of this sulpha drug were examined by using different methods (calorimetry/DSC, simultaneous small- and wide-angle X-ray scattering/SWAXS, freeze-fracture combined with transmission electron microscopy). Of these procedures, freeze-fracture was a powerful method for obtaining unique visual information about the wealth of complex changes in the multilamellar system [23–25].

2. Materials and methods

Synthetic 1,2-dipalmitoyl-*sn*-glycero-3-phosphoethanolamine (DPPE, purity>99%) and 1,2-dipalmitoyl-*sn*-glycero-3-[phospho-*rac*-1-glycerol] (DPPG, Na salt, purity>99%) were purchased from Avanti Polar Lipids, Inc. (Alabaster, Ala, USA). SD (benzenesulfonamide, 4-amino-*N*-2-pyrimidinyl) was obtained from Sigma–Aldrich (Steinheim, Germany; purity>99%) and from Vetranal, Riedel-de Haën, Sigma Aldrich (Copenhagen, Denmark; purity>99.8%). The substances were used without further purification.

Appropriate amounts of the lipids (DPPE and DPPG) were mixed and dissolved in chloroform containing 30 vol.% methanol; then the solution was evaporated at 70 °C. The resulting lipid film was kept in vacuum to remove the residual traces of the solvent. Triple-quartz-distilled deionized water (18.2 MΩ cm; with a Millipore Simplicity 185 filtration system) or Tris buffer (10 mM, pH 7.4) was added to the dried lipid and to the mixture of the dried lipid and SD powder (see below) to yield a lipid concentration of 20 (w/w) %. The sample was heated above the phase transition (65 °C) for 15 min, and then cooled to 5 °C, heated once again to 65 °C and vortexed intensively. This treatment was repeated 20 times to achieve homogeneous dispersions. The concentration of SD varied in a wide range: the molar ratios of SD relative to the lipids (SD/lipids) were 10^{-3}, 10^{-2}, 10^{-1}, and 1.

The DSC measurements were performed with a DSC 2920 instrument (TA Instruments, USA) operated at a heating rate of 1 °C/min in the temperature range from 25 to 70 °C. The DSC curves were recorded in the heating direction. The reference pan was empty. The calorimeter was calibrated by using a pure indium sample (T_{onset}=156.6 °C). The transition points were characterized by the temperature at which the heat-flow curve exhibited a minimal value.

SAXS and WAXS measurements were performed using a modified Kratky Compact camera (Anton Paar, Graz, Austria) equipped with two position-sensitive detectors (M. Braun, Garching, Germany). With this SWAXS camera, simultaneous detection in the small- and wide-angle region was performed. The scattering of Ni-filtered CuKα radiation (λ=1,542 Å) was recorded in the small-angle range from 10^{-3} to 10^{-1} Å^{-1} and in the wide-angle range from 0.2 to 0.3 Å^{-1} of the scattering variable, defined as $s=(2\sin\Theta)/\lambda$, where 2Θ is the scattering angle. The primary beam was line-focused. Thus, the intensity curves of SAXS were corrected with respect to the geometry of the beam profile [26]. The SAXS curves were presented only in a narrower range of the scattering variable where the characteristic changes occurred (from 0.005 to 0.05 Å^{-1}). For the X-ray measurements, the samples were transferred into thin-walled capillaries (Hilderberg, Germany) with a diameter of 1 mm. After centrifugation to remove air bubbles the capillaries were sealed with a two-component synthetic resin and transferred into metal capillary holders that were placed into an aluminium block. This block was positioned directly into the beam line and was used as a thermal incubator for controlled annealing at different temperatures. The X-ray measurements were performed by a heating programme in the phase transition range of each system. After 15 min incubation of the samples at the respective temperatures the exposure took 600 s for detection in the small- and wide-angle X-ray scattering regions. The control SAXS measurements were conducted in the JUSIFA facility (Jülich's user-dedicated small angle scattering facility) at the DORIS synchrotron radiation source in DESY (German Synchrotron, Hamburg), using a selected X-ray beam of 9040 eV corresponding to a wavelength of λ=1.516 Å [27]. The scattering pattern of the vesicles was monitored with a two-dimensional position-sensitive detector, a multiwire proportional counter (MWPC) with 256×256 resolution pixels on 180×180 mm^2 active area.

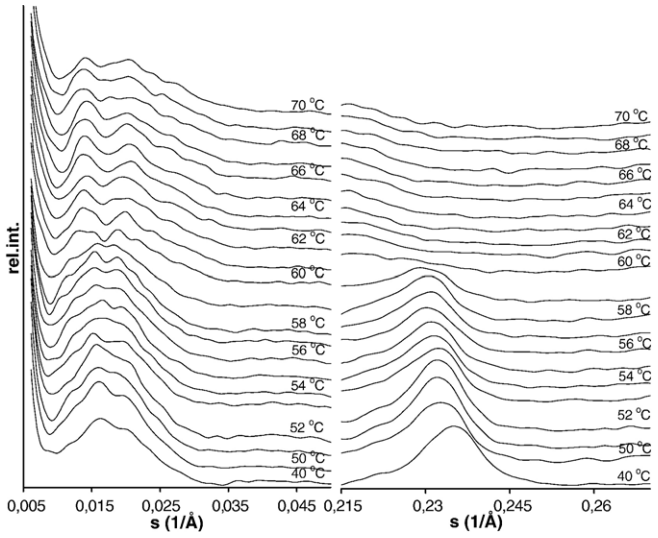

Fig. 2. SAXS and WAXS patterns of the DPPE-DPPG/water system in the gel and in the liquid crystalline phases.

For freeze-fracture, the sample and the gold specimen holders were incubated at the respective temperatures. Droplets of 1–2 μl of the sample were pipetted onto gold holders (also incubated at the desired temperatures) and frozen immediately by plunging them into partially solidified Freon for 20 s and the samples were then stored in liquid nitrogen. Fracturing was performed at −100 °C in a Balzers freeze-fracture device (Balzers AG, Vaduz, Liechtenstein). Replicas of the fractured faces etched at −110 °C were made by platinum-carbon shadowing, then cleaned with a water solution of surfactant and washed with distilled water. The replicas were placed on 200 mesh copper grids and examined in a JEOL JEM-100 CX II electron microscope (Japan).

3. Results

3.1. Structural and morphological characterization of the pure lipid (DPPE-DPPG)/water system

The chain packing and the layer arrangement of the DPPE-DPPG/water vesicle system were studied in the wide temperature range of their gel and liquid crystalline phases (Fig. 2). The changes in WAXS profiles reveal more characteristic differences between the structures formed in the thermally adjacent phases than those in the SAXS patterns. The single Bragg reflection located at 1/4.25 $Å^{-1}$ (40 °C) exhibits nearly hexagonal chain packing in the bilayers. When the temperature is increased, the Bragg reflection shifts continuously to the lower scattering values (up to 1/4.34 $Å^{-1}$) and broadens significantly. These changes extend throughout the investigated temperature domain (from 40 to 60 °C), indicating that the chain melting process is in progress. The Bragg peak disappears at 60 °C due to the phase transition between the gel and liquid crystalline phases. Nevertheless, the thermogram shows a sharp transition signal at 60.5 °C as can also be seen in Fig. 4 and as was reported in our earlier paper [22]. Therefore, we can conclude that the hydration forces between the charged DPPE and DPPG molecules play a dominant role during the phase transition, which is accompanied by only a reduced effect of the lateral lipid arrangement. The SAXS patterns exhibit complex forms and they are temperature-dependent. In the temperature domain of the gel phase the main Bragg peak is located at 1/63 $Å^{-1}$ and an additional peak on its right shoulder emerges at 1/50 $Å^{-1}$. At the phase transition a change only appears in the curves, namely the shape of the diffractograms is modified in the temperature domain between 59 and 60 °C. The most diffuse character of the SAXS curve appears at 59 °C. This is nearly the same temperature as that at which the WAXS profile of the chain packing ceases to exist. Above this value the main peak is shifted to 1/67 $Å^{-1}$ indicating a larger characteristic distance in the layer system. The additional peak in the 1/56–1/43 $Å^{-1}$ interval of scattering is presumably the sum of several

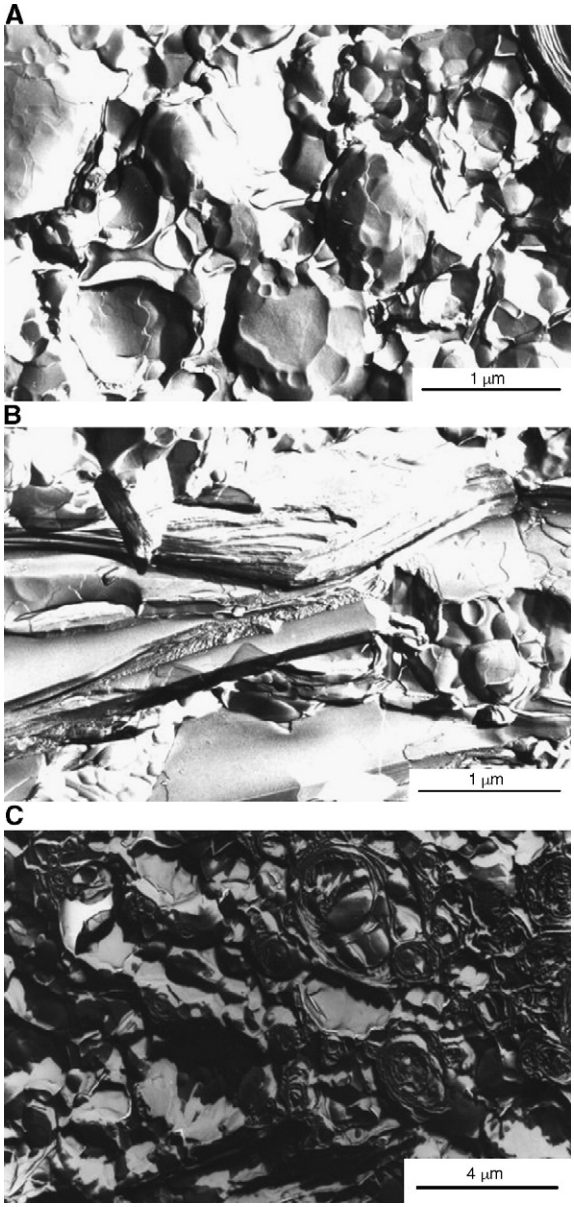

Fig. 3. Characteristic surface morphology of the DPPE-DPPG/water vesicles in the gel phase at 50 °C (A), occasionally stacks of parallel layers appear at 50 °C (B), characteristic surface morphology in the liquid crystalline phase at 62 °C (C).

reflections. The complex, diffuse shape of the SAXS patterns of both phases may be a superposition of overlapping Bragg peaks but it is not possible to unambiguously deduce a structural description. The electron microscopy study after the freeze-fracture procedure provides more information on the existence of non-correlated layer structures in the gel and liquid crystalline phases. Both spherical and multilamellar creations can be recognized in the surface morphology of the gel phase formed at 50 °C. Typically, fractured giant vesicle and smaller spherical forms are present as shown in Fig. 3A. Occasionally, multilamellar parts appear to consist of a very large number of stacks of lipid multilayers without any curvature (Fig. 3B). In the liquid crystalline phase (at 62 °C) the size of the liposomes is highly heterodispersive, as observed in Fig. 3C. Between some giant vesicles a great number of smaller spherical forms are visible. Some of them are embedded into the inner parts of other larger liposomes. The non-regular layer arrangement is typical of both phases, and other liotropic structural formations (cubic, hexagonal), even in locally, cannot be recognized.

3.2. Effects of sulfadiazine on the DPPE-DPPG/water system

The concentration dependence effect of sulfadiazine (SD) on the DPPE-DPPG/water system can be comprehensively shown by presenting their DSC thermograms (Fig. 4) detected in a wide SD/lipid molar ratio range from 10^{-3} to 1. In the absence of SD molecules, the pure lipid/water system undergoes a single phase transition between the gel and liquid crystalline phases at 60 °C as shown in the upper thermogram in Fig. 4. However, this peak is broadened, indicating that there is a complex behaviour in the transition of this lipid mixture, which originates from the formation of two types of domains with different DPPE/DPPG lipid ratios. In the low SD concentration regime (10^{-3}–10^{-1} SD/DPPE-DPPG), a phase separation appears which results in only a minor change in enthalpy. A

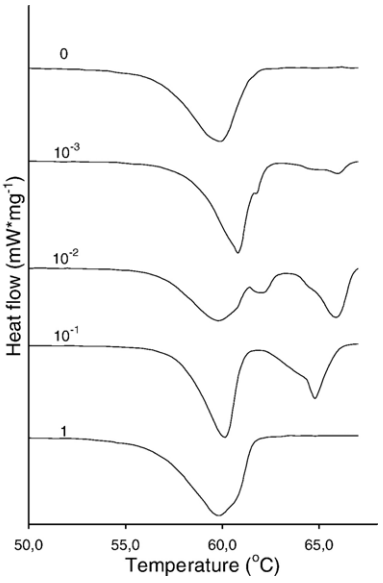

Fig. 4. DSC curves of the DPPE-DPPG/water systems with different SD/lipid ratios marked on each curve.

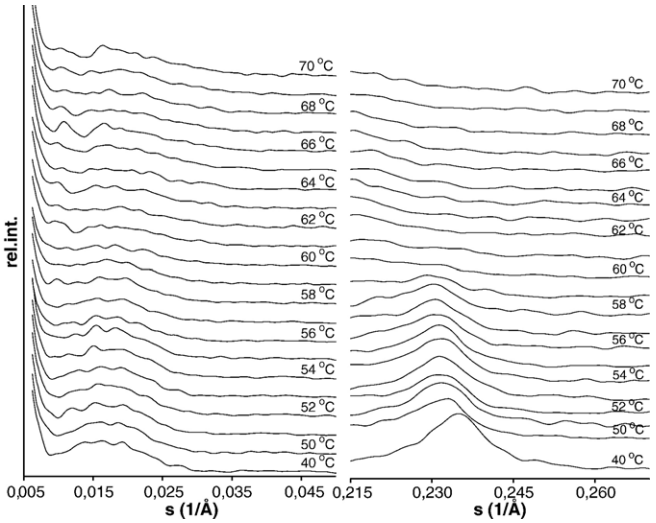

Fig. 5. SAXS and WAXS patterns of the SD(99%)/DPPE-DPPG/water system with 10^{-1} SD/lipid ratio in the temperature domain from 40 °C to 70 °C.

right shoulder emerges from the transition signal and it becomes more intensive at higher SD concentrations. Moreover, the significant first transition peak is accompanied by a second transition located at approx. 65 °C. The location of the second transitional signal was not only changed at different SD concentration, but also in samples originating from repeated preparation. In the shape and location of the signal the more clearly expressed changes were observed by changing the quality of SD at 10^{-1} SD/lipid ratio. If the purity of SD was increased from 99% (Sigma product) to 99.8% (Vetranal product) the location of the second transition was decreased from 65 °C to 62 °C. Upon the addition of SD (1 SD/DPPE-DPPG, where the SD molecules cannot be considered as guest molecules but rather host molecules), the shape of the thermogram completely changed; only one complex peak was detected.

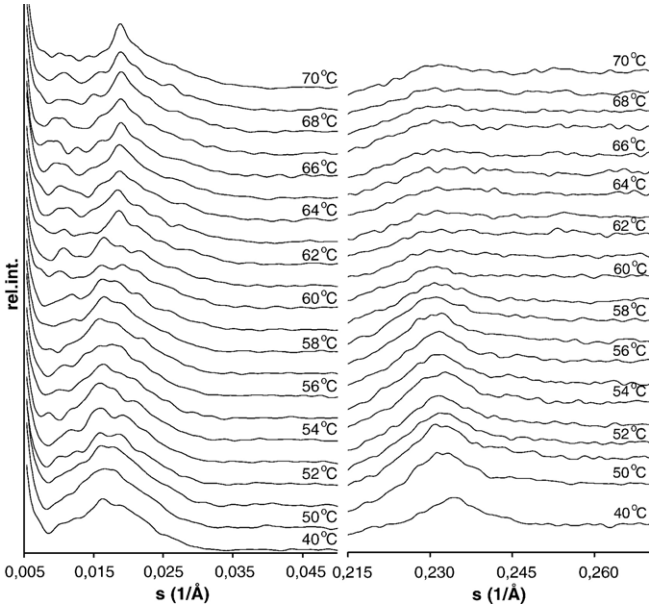

Fig. 6. SAXS and WAXS patterns of the SD(99.8%)/lipid/water system with 10^{-1} SD/lipid ratio in the temperature domain from 40 °C to 70 °C.

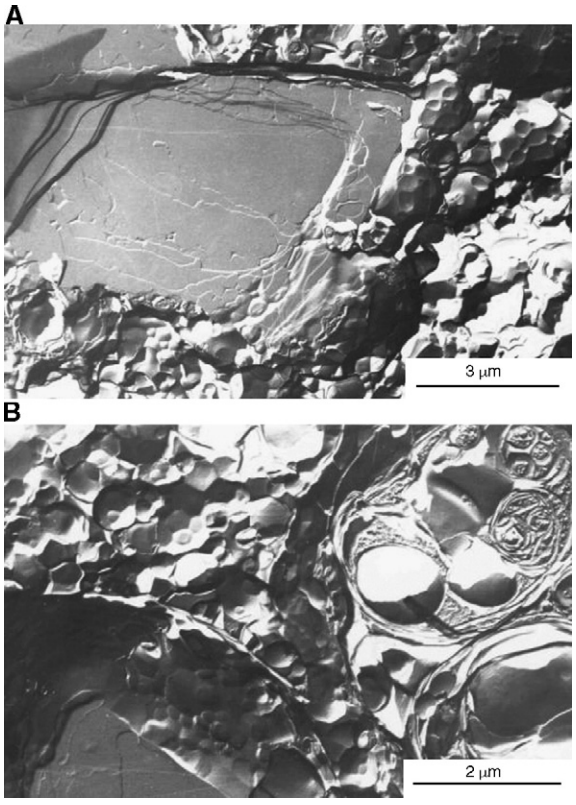

Fig. 7. Characteristic surface morphologies of the SD(99%)/DPPE-DPPG/water system with 10^{-1} SD/lipid ratio at 50 °C. Stacks of layers (A) and smaller vesicles of heterogeneous size embedded in large vesicles (B).

Now our attention is focused on the formation of the second transitional signal in the case of the system doped with 10^{-1} SD/lipid ratio. Simultaneous small- and wide-angle X-ray scattering (SWAXS) measurements were made in order to follow the changes in the chain packing and also in the layer arrangement from 40 °C to 70 °C. The characteristic parts of the SAXS patterns and the WAXS profiles of the system doped with SD (99%) are shown in Fig. 5. Only moderate changes in the SAXS curves appeared relative to the patterns of the pure lipid/water system. The most diffuse scattering profile appears at the same temperature (60 °C), where the first DSC signal is located, therefore indicating that the strongest destruction in the layer arrangement occurs at this temperature. The complex and diffuse character of the SAXS curves remains up to 64 °C. Above this temperature (up to 70 °C), further changes can be observed in the scattering curves showing further alterations in the layer structure. In the changes of the WAXS profiles only one characteristic temperature can be recognized, namely 60 °C, where the broadened Bragg peak of the lipid packing disappears. There is great similarity between the temperature-dependent formation of the Bragg profiles of the system doped with SD and that of the pure lipid system (Figs. 5 and 2). However, the SWAXS curves of the doped system are more diffuse, and the shapes of their peaks are significantly more broadened than those in the case of the pure lipid system. This indicates that the presence of SD molecules causes severe destruction in both the inter- and inner-layer structures. The SD with higher purity (99.8%) affects the system in the same way as the lower purity SD (99%) does (Fig. 6). That is to say, there are changes in the SAXS profiles at two temperatures (60 °C and 62 °C) and in the WAXS profiles at only one (60 °C). On the other hand, there are some special differences; the peaks exhibit sharper forms in the SAXS curves while the WAXS profiles are more smeared than those of the system with lower-purity SD. It is worth mentioning that the characteristic temperatures observed in the SAXS profiles (60 °C and 65 °C in the case of 99% SD purity, and 60 °C and 62 °C in the case of 99.8% SD purity) are in full agreement with the thermograms.

Significant changes in the morphology can be observed in the presence of SD (99%). The system with 10^{-1} SD (99%)/lipid ratio was quenched from three characteristic temperatures (50, 62, and 70 °C) corresponding to the gel phase, the transitional state between the two transitions detected by the DSC and SAXS methods, and the liquid crystalline phase, respectively. In the gel phase, giant vesicles appear more rarely than in the case of the absence of SD. Also, large cohesive parts are formed between small-size vesicles and multilamellar formations similar to those observed in the pure DPPE-DPPG system (Fig. 7A). Domains of stacks of parallel layers with lateral extension of several micrometers are frequently visible. The other parts of the sample consist of giant vesicles in which spherical forms of various sizes are embedded (Fig. 7B). At 62 °C, the morphology shows great similarity to that formed in the lower temperature domain as giant blocks consisting of a huge number of multilayers are embedded between the destroyed vesicles. Differences, however, can be

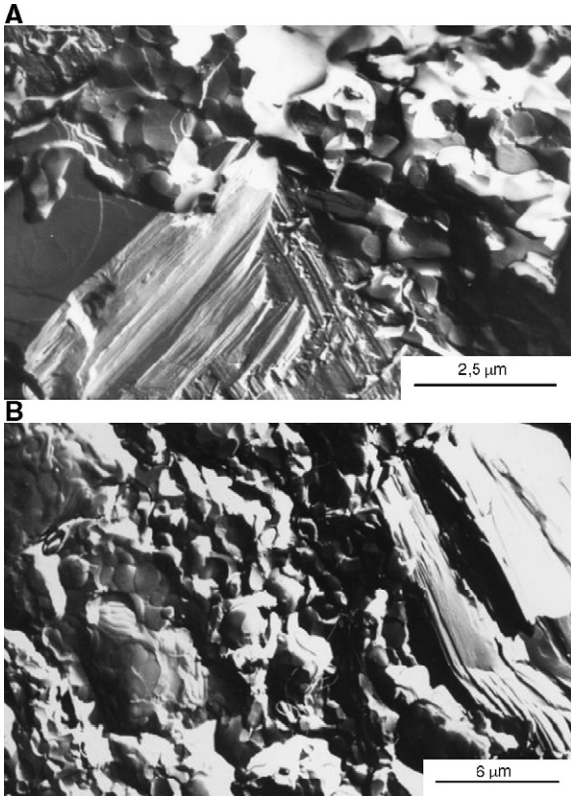

Fig. 8. Typical surface morphology of the SD(99%)/DPPE-DPPG/water system with 10^{-1} SD/lipid ratio at 62 °C; giant stacks of parallel layers with "melted-like" (A) and heterodisperse irregular vesicles (B).

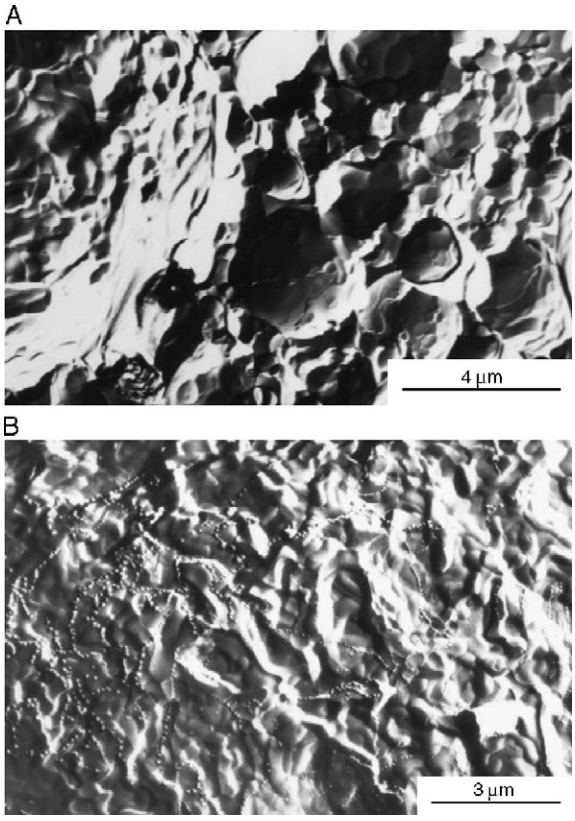

Fig. 9. Surface morphology of the SD(99%)/DPPE-DPPG/water system with 10^{-1} SD/lipid ratio at 70 °C; destroyed vesicles (A) and crinkled extended layer formations (B).

observed in the heterodisperse and irregular vesicles, which exhibit more "melted-like" fractured surfaces and destroyed, non-spherical forms are present as is shown in Fig. 8A and B. At 70 °C, the vesicular forms reappear, and also a higher proportion of giant liposomes (Fig. 9A). However, the other parts of the sample do not consist of any spherical forms, and smoother surfaces alternating with more crinkled layer parts can be observed (Fig. 9B). It is obvious that the stacks of multilayers do not exist in the high-temperature domain.

4. Conclusion

The great variety of both the structural and morphological formations originate from the unusual feature of the DPPE-DPPG/water system [19]. The pure lipid system shows non-ideal miscibility and the segregation of DPPE domains was found above 0.9 DPPE molar ratio (relative to DPPE-DPPG), but the system exhibits inhomogeneous domain formation, even at 0.8 DPPE molar ratio. Adding sulfadiazine to the system destroys the layer arrangement and the chain packing. The drastically broadened WAXS profiles extending into the investigated temperature interval show a strong decrease of the cooperativity of the first transition. These features indicate the dominance of the hydration forces between the guest and the lipid molecules. Moreover, the presence of any impurities (especially charged ones) may play an important role in domain formation [28–31]. DPPE and DPPG are conical-shaped molecules. The cross-sectional areas of their head groups are about 38 and 70 $Å^2$, respectively, while their chain cross-sectional area extends only to 20 $Å^2$ [32]. Therefore, their self-organisation results in non-regular vesicle formations. The localisation of SD molecules to the head-group region of lipids may reduce the lateral extension of the coherent domains whereby more diffuse WAXS profiles can appear than in the pure lipid system. The SD molecules with a higher grade of purity (99.8%) are dispersed more homogeneously in the lipid bilayers than in the case of those of lower purity (99%). In this way, a more extensive broadening may occur in the WAXS profiles. Concomitantly, sharper SAXS profiles appear corresponding to a more regular layer arrangement. Hence, more broadened WAXS and sharper SAXS profiles appeared in Fig. 6 (99.8% SD) than in Fig. 5 (99% SD), respectively.

We can conclude that the SD molecules are located more inhomogeneously in the gel phase than in the liquid crystalline phase. In the high-temperature domain, where the chain cross-sectional area of both lipids is expanded to 50 $Å^2$ and their shapes become cylindrical (they are slightly conical, but in other directions), the formation of a laterally extended layer structure is expected. The metastable creations induced by the locally enriched SD molecules may only cease to exist in a higher temperature domain resulting in a second transition, dependent on conditions (purity, presence or absence of buffer system), so that a more correlated layer structure can form in the high-temperature domain. These model investigations suggest that SD predominantly affects the lipids in their polar head group regions and may disturb large molecules like membrane peptides embedded in the outer leaflet of the membrane by polar interactions.

Acknowledgements

This work was supported by the Hungarian Scientific Fund OTKA (Bóta, T 43055) and a German–Hungarian research project. We thank Dr. G. Goerigk for scientific and technical support at the synchrotron station, Mrs. T. Kiss and Mrs. E. Tóth for technical assistance with the freeze-fracture and DSC measurements, respectively. The SAXS measurements were supported by Contract RII3-CT-2004-506008 of the European Community at DESY/HASYLAB (Hamburg, Germany).

References

[1] A.B.A. Boxall, L.A. Fogg, P.A. Blackwell, P. Kay, E.J. Pemberton, A. Croxford, Veterinary medicines in the environment, Rev. Environ. Contam. Toxicol. 180 (2004) 1–91.
[2] A.B.A. Boxall, D.W. Kolpin, B. Halling-Sorensen, J. Tolls, Are veterinary medicines causing environmental risks? Environ. Sci. Technol. (2003) 286–294.
[3] B. Halling-Sorensen, G. Sengelov, F. Ingerslev, L.B. Jensen, Reduced antimicrobial potencies of oxytetracycline, tylosin, sulfadiazin, streptomycin, ciprofloxacin, and olaquindox due to environmental processes, Arch. Environ. Contam. Toxicol. 44 (2003) 7–16.
[4] R. Hirsch, T. Ternes, K. Haberer, K.L. Kratz, Occurrence of antibiotics in the aquatic environment, Sci. Total Environ. 225 (1999) 109–118.
[5] S. Hida, M. Yoshida, I. Nakabayashi, N.N. Miura, Y. Adachi, N. Ohno, Anti-fungal Activity of sulfamethoxazole toward *Aspergillus* species, Biol. Pharm. Bull. 28 (5) (2005) 773–778.

[6] A. Wehrhan, Fate of veterinary pharmaceuticals in soil: an experimental and numerical study on the mobility, sorption and transformation of sulfadiazine, PhD Thesis, Agrosphere Institute, Research Centre Jülich, 2006.
[7] P.L. Yeagle, The Membranes of Cells, Academic Press, Inc., London, 1993, pp. 43–66.
[8] H.R. Petty, Molecular Biology of Membranes, Plenum Press, New York, 1993, pp. 7–20.
[9] S.R. Conrad, M.J. Howard, R.C. Garrison, S. Winters, D.A. Henderson, The effects of daptomycin on chemical composition and morphology of *Staphylococcus aureus*, Proc. Okla. Acad. Sci. 78 (1998) 15–22.
[10] M. Pappalardo, D. Milardi, D. Grasso, C. La Rosa, Phase behaviour of polymer-grafted DPPC membranes for drug delivery systems design, J. Therm. Anal. Calorim. 80 (2005) 413–418.
[11] A. Bertoluzza, S. Bonora, G. Fini, O. Francioso, M.A. Morelli, Interaction of bipyridilium herbicides with model membranes, Chem. Phys. Lipids 75 (1995) 137–143.
[12] A. Tahir, C. Gabrielle-Madelmont, C. Betrencourt, M. Ollivon, P. Peretti, A differential scanning calorimetry study of the interaction of Lasalocid antibiotic with phospholipid bilayers, Chem. Phys. Lipids 103 (1999) 57–65.
[13] P. Laggner, K. Lohner, Liposome phase systems as membrane activity sensors for peptides, in: J. Katsaras, T. Gutberlet (Eds.), Lipid Bilayers. Structure and Interactions, Springer, Berlin, 2000, pp. 233–264.
[14] K. Lohner, Development of Novel Antimicrobial Agents: Emerging Strategies, Horizon Scientific Press, Wymondham, 2001, pp. 149–165.
[15] A. Gürsoy, Liposome-encapsulated antibiotics: physicochemical and antibacterial properties, a review, S.T.P. Pharma Sci. 10 (4) (2001) 285–291.
[16] J.B.G. Kwapinski, S.G. Bradley, E.R. Brown, P.R. Burton, H. Fraenkel-Conrat, N. Kordová, W.M. O'Leary, F.J. Reithel, M.R.J. Salton, R. Storck, E.E. Woodside, Molecular Microbiology, John Wiley and Sons, New York, 1974, pp. 402–408.
[17] W.M. O'Leary, S.G. Wilkinson, in: C. Ratledge, S.G. Wilkinson (Eds.), Gram-Positive Bacteria, Microbial Lipids, vol. 1, Academic Press, London, 1988, pp. 117–201.
[18] S.G. Wilkinson, in: C. Ratledge, S.G. Wilkinson (Eds.), Gram-Positive Bacteria, Microbial Lipids, vol. 1, Academic Press, London, 1988, pp. 299–488.
[19] K. Lohner, A. Latal, G. Degovics, P. Garidel, Packing characteristics of a model system mimicking cytoplasmic bacterial membranes, Chem. Phys. Lipids 111 (2001) 177–192.
[20] K. Lohner, E.J. Prenner, Differential scanning calorimetry and X-ray diffraction studies of the specificity of the interaction of antimicrobial peptides with membrane-mimetic systems, Biochim. Biophys. Acta 1462 (1999) 141–156.
[21] E. Urbán, A. Bóta, B. Kocsis, K. Lohner, Distortion of the lamellar arrangement of phospholipids by deep rough mutant lipopolysaccharide from *Salmonella minnesota*, J. Therm. Anal. Calorim. 82 (2005) 463–469.
[22] E. Urbán, A. Bóta, B. Kocsis, Non-bilayer formation in the DPPE-DPPG vesicle system induced by deep rough mutant of *Salmonella minnesota* R595 lipopolysaccharide, Colloids Surf., A Physicochem. Eng. Asp. 48 (2006) 106–111.
[23] S.W. Hui, Freeze fracture studies of membranes lipids, Electron Microsc. Rev. 1 (1988) 351–370.
[24] H.W. Meyer, W. Richter, Freeze-fracture studies on lipids and membranes, Micron 32 (2001) 615–644.
[25] Á. Oszlánczi, Cs. Novák, E. Klumpp, Effect of sulfadiazine on biological membranes, J. Therm. Anal. Calorim. 82 (2005) 457–462.
[26] O. Glatter, Convolution square root of band-limited symmetrical functions and its application to small-angle scattering data, J. Appl. Crystallogr. 14 (1981) 101–108.
[27] H.-G. Haubold, K. Gruenhagen, M. Wagener, H. Jungbluth, H. Heer, A. Pfeil, H. Rongen, G. Brandenberg, R. Moeller, R. Matzerath, P. Hiller, H. Halling, JUSIFA — a new user-dedicated ASAXS beamline for materials science, Rev. Sci. Instrum. 60 (7) (1989) 1943–1946.
[28] R.P. Rand, V.A. Parsegian, Hydration forces between phospholipid bilayers, Biochim. Biophys. Acta 988 (1989) 351–376.
[29] M.E. Loosley-Millman, R.P. Rand, V.A. Parsegian, Effects of monovalent ion binding and screening on measured electrostatic forces between charged phospholipid bilayers, Biophys. J. 40 (1982) 221–232.
[30] P. Garidel, A. Blume, Miscibility of phosphatidylethanolamine–phosphatidylglycerol mixtures as a function of pH and acyl chain length, Eur. Biophys. J. 28 (2000) 629–638.
[31] P. Garidel, C. Johann, A. Blume, Thermodynamics of lipid organization and domain formation in phospholipid bilayers, J. Liposome Res. 10 (2000) 131–158.
[32] J. Wilschut, D. Hoekstra, Membrane Fusion, Marcel Dekker, Inc., New York, USA, 1991, p. 8.